Nitrogen-doped porous carbon prepared from liquid carbon precursor for CO2 adsorption

Article *in* RSC Advances · May 2015

DOI: 10.1039/C5RA08014B

3 authors, including:

Donghai Lin
Shanghai Polytechnic University
70 PUBLICATIONS **672** CITATIONS

SEE PROFILE

Weixing Chen
University of Alberta
136 PUBLICATIONS **5,769** CITATIONS

SEE PROFILE

RSC Advances

PAPER

View Article Online
View Journal | View Issue

Cite this: *RSC Adv.*, 2015, **5**, 45136

Nitrogen-doped porous carbon prepared from a liquid carbon precursor for CO_2 adsorption

Xiaotian Zhang, Donghai Lin and Weixing Chen*

Received 1st May 2015
Accepted 5th May 2015

DOI: 10.1039/c5ra08014b

www.rsc.org/advances

We report a new carbonaceous material derived from a liquid precursor, polyethylenimine (PEI) by chemical activation using KOH. The PEI-derived activated carbon possesses typical microporosity with a high specific surface area. It also features rich nitrogen content and various nitrogen functional groups. It was found that at 1 bar the CO_2 uptake of these PEI-derived carbons was 4.9–5.7 mmol g^{-1} at 0 °C and 2.9–3.7 mmol g^{-1} at 25 °C. Specifically, the CO_2 adsorption capacity of the carbon activated at 600 °C was the highest, being 5.67 mmol g^{-1} at 0 °C, atmospheric conditions. The PEI-derived carbons also exhibit very good stability during multi-cycle adsorption–desorption tests and a high selectivity of CO_2 over N_2 at 25 °C.

1. Introduction

Concerns about excessive CO_2 emission (such as global warming) have led to research on many promising solutions to the problem.[1,2] The current technology used to reduce CO_2 emission in power plants, a major source of CO_2 emission, is liquid amine-based absorption.[3] However, disadvantages such as limited absorption capacity and high-energy consumption have urged us to look for more cost-effective methods. Recently, materials based on zeolites,[4–6] mesoporous silica,[7–9] metal–organic frameworks (MOFs),[10–12] covalent–organic frameworks (COFs)[13] and porous carbons,[14,15] especially N-enriched porous carbons[16–21] have been reported for CO_2 adsorption and storage. Among them, zeolites are very sensitive to moisture, impregnated mesoporous materials suffer instability during cyclic tests, and MOFs/COFs are expensive and complex upon synthesis. Carbon-based adsorbents, however, possess high thermal/chemical stability, high surface area, large adsorption capacity and reasonable cost. Therefore they are one of the most promising materials for CO_2 capture.

For N-enriched porous carbons, CO_2 adsorption could be facilitated by the presence of microporous structure and strong interaction between the CO_2 molecules with the framework (especially N-containing groups) through H-bonding or dipole–quadrupole interactions.[2] As for pore development, KOH activation is highly desirable because it develops large amount of micropores with high surface area.[22,23] In 2011 Sevilla *et al.*[24] further demonstrated how severe (KOH four times the precursor) and mild activation conditions (KOH two times the precursor) at various temperatures affect the texture of the porous carbons and their CO_2 adsorption ability. Whereas the mildly-activated carbons showed small surface area (1300 m^2 g^{-1}) and narrow micropores (<1 nm), the severely-activated ones showed greater surface area (>2000 m^2 g^{-1}) and larger pore sizes (1–3 nm). However, the former condition exhibited a better CO_2 uptake primarily due to the presence of narrow micropores (<1 nm), while the surface area is playing a less significant role. Moreover, the porous structure and required KOH amount are closely related to carbon precursors, since many activated carbons[24–26] required different KOH/C ratio for optimized CO_2 adsorption. Therefore it is possible to prepare activated carbons using low KOH/C ratio from carefully selected carbon precursors.

Branched polyethylenimine (PEI, Fig. 1) is inexpensive, non-toxic and widely used for DNA transfection in cell studies.[27] PEI also has abundant amino groups, as a result it was employed as an impregnating agent for mesoporous silica, such as MCM-41,[28] SBA-15 [29] and MCF[30,31] for the sake of CO_2 adsorption. However, considerable leaching of the amines may be a major drawback for the use of PEI-impregnated mesoporous silica sorbents for CO_2.[5] For example, it has been reported that the performance of a typical PEI/silica material dropped ~30% after only 6 cycles.[32] Therefore in this paper, we explored a one-step KOH activation method using PEI as carbon precursor. To our best knowledge, this is the first time that PEI is employed to produce activated carbon material and a liquid carbon precursor has been used. The synthesis process is facile. Owing to its liquid property, PEI could be completely mixed with KOH at the early stage, which results in well-developed porous structure as well as rich nitrogen content at very low KOH/C ratio. Considering the corrosive nature and comparably high price of KOH, this material is much more cost-saving in terms of synthesis and facility. In this study, PEI-derived carbons were carefully examined in terms of pore structures and N-containing functionalities. The contributions of microporosity and N-containing groups to CO_2 adsorption capacity were discussed.

Department of Chemical and Materials Engineering, University of Alberta, Edmonton, T6G 2G6, Canada. E-mail: weixing.chen@ualberta.ca

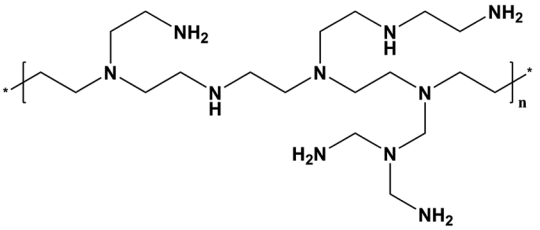

Fig. 1 Schematic diagram for branched polyethylenimine (PEI).

2. Experimental

2.1 Preparation of PEI-derived carbon

The PEI-derived carbon was synthesized *via* a carbonization–activation process by using KOH as an activation agent. Commercialized PEI, purchased from MP Biomedicals, was used as carbon precursor without any further purification. KOH (pellet) was purchased from Fisher Scientific Canada. In a typical synthesis, 4 g viscous PEI was first dissolved in 50 mL ethanol and magnetically stirred for 15 min until a clear solution was obtained. Then 2 g KOH was added to the solution followed by 6 hours of magnetic stirring with a speed of 300 rpm. After fully mixed, the mixture was transferred into a rectangular alumina boat and dried in an oven at 80 °C for 12 hours. The after-dry mixture returned to a viscous state due to evaporation of solvent. The boat was allowed to cool down to room temperature and placed into a horizontal quartz tube. The tube was initially vacuumed to a pressure below 30 Pa before N_2 (purity > 99.998%) was introduced at a steady flow rate of 100 cm^3 min^{-1}. After purging for 1 h, the furnace was ramped up to activation temperature with a heating rate of 3 °C min^{-1} and held for 3 hours. After activation, the furnace was allowed to cool down naturally. Then the samples were taken out and washed with copious Milli-Q water several times until the pH was ~7. The washed carbons were dried again at 90 °C for over 24 hours. The samples after synthesizing were denoted as C-*x*, where *x* is the activation temperature. The dried samples were ~490 mg for C-500, ~210 mg for C-600 and ~130 mg for C-700.

For acid neutralization process, samples were first treated with excess amount of 37 wt% concentrated HCl solution for 24 hours, followed by copious Milli-Q water wash until the pH was ~7. The HCl-treated carbons were sent in oven and dried at 90 °C for 24 hours.

2.2 Characterization

The morphologies of the samples were examined by scanning electron microscopy (SEM) using a JAMP-9500F system (JEOL, Tokyo, Japan) under 15 kV. Transmission electron microscopy (TEM) images were received from a JOEL 2010 system with an operating voltage of 200 kV. N_2 adsorption–desorption results were obtained at 77 K by an Autosorb-1 system (Quantachrome). Every sample (~30 mg) was outgassed under high vacuum at 150 °C for over 4 h before test. The specific surface area was calculated by Brunauer–Emmett–Teller (BET) method based on data points in the partial pressure range of 0.03–0.1, within which the linear correction coefficient was >0.9999. This range is lower than the usual range (P/P_0 = 0.1–0.3) because their microporous properties render capillary condensation at lower relative pressure.[33] The pore size distribution was determined using quenched-solid density functional theory (QSDFT) method assuming a slit/cylindrical pore model. For characterization of chemical properties, infrared spectrum was recorded with a Nicolet 8700 Fourier transformation infrared (FTIR) spectrometer (Thermal Scientific), the scanning range was between 500 and 4000 cm^{-1}, with a resolution of 1.93 cm^{-1} and 128 scans per test. X-ray photoelectron spectroscopy (XPS) was carried with an AXIS 165 system (Kratos Analytical Ltd., UK) using a monochromated Al Kα excitation source.

2.3 CO_2 adsorption

CO_2 adsorption capacity at different temperatures was collected by Autosorb iQ (Quantachrome). Before adsorption every sample (~50 mg) was outgassed under high vacuum at 150 °C for over 4 h before test. The temperature control was performed by a tube furnace. Adsorption–desorption multi-cycle stability was tested by thermalgravimetric analysis (TGA). A sample of ~5 mg was placed in a platinum crucible in a TGA machine (SDT Q600, TA Instrument). The sample was first heated to 105 °C under N_2 environment for 30 min to be fully desorbed, and then equilibrated at 25 °C. During adsorption, the sample was exposed to a desired mixed gas (100 mL min^{-1}, 95% CO_2 with balance of N_2, CO_2 concentration cannot reach 100% due to facility limitation). The sample was then kept at this condition for 1 h for adsorption. Once the adsorption is completed, the gas was switched from mixed gas to pure N_2 (100 mL min^{-1}), and the sample was heated to 105 °C for thorough desorption. The weight change profile measured was determined to be the amount of CO_2 adsorption. This process then was repeated for 30 times.

3. Results and discussion

3.1 Porous structure

Fig. 2 shows microscopic images of a typical sample (C-600). As could be seen in Fig. 2a, the activated carbon demonstrates a generally smooth surface decorated with macropores. However, a sponge-like structure was revealed in the cross-sectional morphology of Fig. 2b. The TEM image of PEI-derived carbon in Fig. 2c shows typical amorphous structure of activated carbon. Worm-like micropores composed of deformed graphitic layers can be observed in HR-TEM image of Fig. 2d.

Nitrogen adsorption–desorption analysis was also performed to characterize the porous structure of the PEI-derived carbon. Fig. 3 shows isotherms of PEI-derived carbons activated at different temperatures. According to the IUPAC,[34] all three isotherms in Fig. 3a are type I. The significant amount of adsorption at low pressures indicated the existence of large amount of micropores. The uptrend at high pressures is consistent with the macropores observed in microscopic images. In terms of the effect of the activation temperature, the main difference lies at the positions of knee points, which

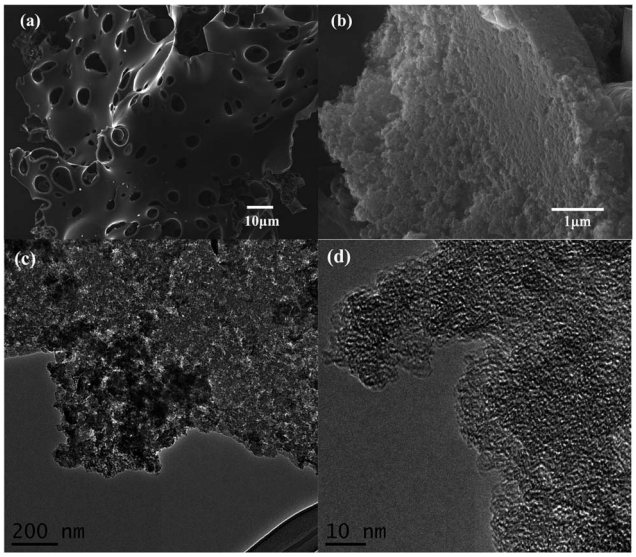

Fig. 2 SEM and TEM images of PEI-derived carbon: (a) surface; (b) cross-section; (c) TEM image; (d) HR-TEM image.

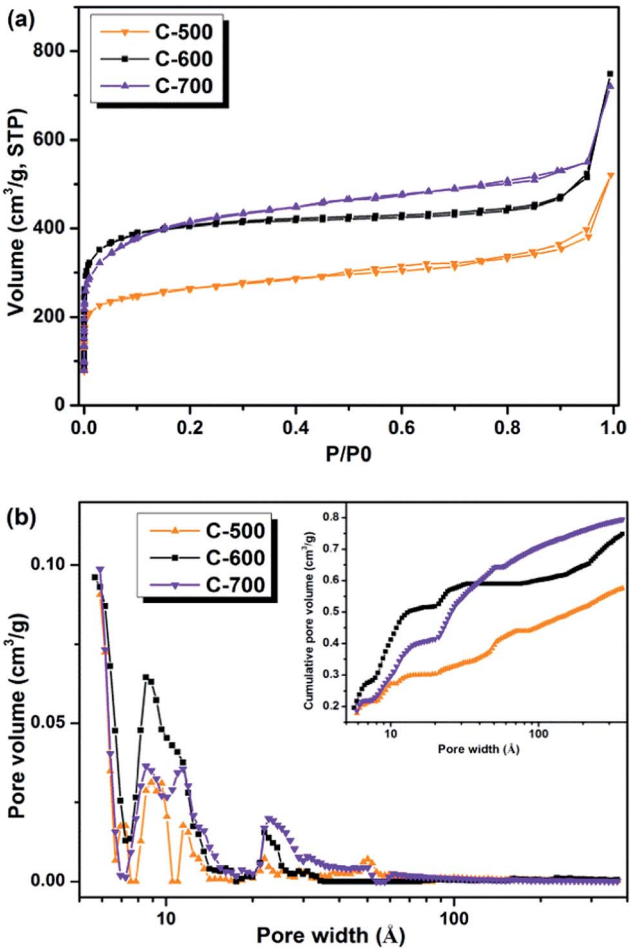

Fig. 3 Nitrogen adsorption–desorption isotherms and pore size distribution of PEI-derived carbon samples under different temperature.

indicates different amount of micropores. A closer look is presented by portraying pore size distributions of different samples in Fig. 3b. Obviously, most of pores are micropores with major peaks centered at ~10 Å, which are best pore sizes for CO_2 adsorption according to literature.[35,36] Additionally, the number of mesopores (20–50 Å) keeps increasing from C-500 to C-700. Statistic pore characteristics of different samples are listed in Table 1. From the results, the total volume increases with increasing activation temperature. However, micropore volume, micropore volume percentage and <1 nm pore volume peak at 600 °C (sample C-600) have the best developed microporosity, with BET surface area of 1540 $m^2\ g^{-1}$, total pore volume of 0.75 $cm^3\ g^{-1}$ and micropore volume of 0.52 $cm^3\ g^{-1}$.

3.2 Chemical characterization

Surface functional groups and chemical composition of the PEI-derived carbons were analyzed by FTIR in Fig. 4a and XPS in Fig. 5, respectively. As presented in Fig. 4a, most peaks in the spectra could be clearly resolved. The two top spectra are similar: the weak band at 3450 cm^{-1} is assigned to O–H (from absorbed water and/or hydroxyl groups).[37] The broad band at 3200 cm^{-1} is due to N–H symmetric stretching vibration.[38,39] A doublet at 2898 cm^{-1} and 2830 cm^{-1} is attributed to CH stretching vibration of $-CH_2-$.[40] As is shown in Fig. 1, these groups come from the original structure of PEI. The next two weak but distinct bands at 2351 cm^{-1} and 2200 cm^{-1} are reported to result from absorbed CO_2.[41] The range from 1800 cm^{-1} to 600 cm^{-1} is often called the fingerprint region and difficult to analyze in detail. However, several obvious bands could still be identified. Two strong bands at 1585 cm^{-1} and ~1300 cm^{-1} are attributed to C=C/C–N stretching and C–H bending,[42] respectively. A weak band of frequency slightly higher than 1585 cm^{-1} is referred to be C=O bond (1660 cm^{-1}). The broad band at 780 cm^{-1} can be assigned to N–H wagging of the secondary amines.[43] The bottom signal (C-700) is different. Generally, the signal is weaker, indicating a smaller amount of functional groups. This implies that a lot of thermally-instable functional groups were eliminated at 700 °C. In addition, instead of 1300 cm^{-1}, C-700 has a band at 1136 cm^{-1}, which is attributed to C–N bonds. The disappearance of C–H peak may results from strong carbonization process at higher temperature. The carbonization mechanism of PEI was hypothesized in Fig. 4b, which is similar to carbonization of polyacrylonitrile (PAN).[18,44] At low temperature, the polymers undergo a dehydrogenation process, which leads to cyclization inside the polymer framework. This cyclization step helps preserve the volatile species. As the temperature increases, the framework gradually aromatizes and further crosslinks to form the carbon monolith embedded with nitrogen atoms.

Elemental analysis and quantitative determination of nitrogen-related functional groups is shown in Table 2 and Fig. 5. Sample C-500 has the highest N content, which is 11.1%. At 600 °C this value dropped about half, to 6.9%. These two samples could be considered nitrogen-rich. For C-700, the N content is only 2.7%. The N content decreases quickly with

Table 1 Porous structure of PEI-derived carbon and their CO_2 capture performance

Sample	BET surface area[a] ($m^2\ g^{-1}$)	Total pore volume[b] ($cm^3\ g^{-1}$)	Micropore volume[c] ($cm^3\ g^{-1}$)	Micropore volume percentage[d]	<1 nm pore volume[c] ($cm^3\ g^{-1}$)
C-500	978	0.58	0.30	52%	0.27
C-600	1540	0.75	0.52	69%	0.41
C-700	1538	0.79	0.41	52%	0.30

[a] BET surface area obtained using BET method at $P/P_0 = 0.03$–0.1. [b] Total pore volume at $P/P_0 = 0.995$. [c] Micropore and <1 nm pore volume obtained from QSDFT slit/cylindrical pore model. [d] Micropore volume percentage was obtained as micropore volume/total pore volume.

increasing activation temperature. As for specific nitrogen functionality, N 1s spectra with resolved peaks are given in Fig. 5b. It is obvious that three main peaks could be found in all samples. The signal at 398.0 eV is assigned to pyridine N (N-6), the one at 400.0 eV to pyrrole and imine, amine, imide (N-5), and the one at 401.5 eV to quaternary N (N-*Q*). The two small peaks at higher binding energy (403.3 eV, 405.1 eV) are attributed to oxidized pyridine N oxide (pyridine-N-ox) and N oxide (N-ox).[45] N-5 is the dominant nitrogen species for all samples, which is mostly resulted from pristine PEI structure (Fig. 1). N-6 contribution decreases as activation temperature increases, which was also observed in ref. 23. On the other hand, N-*Q* and oxidized N contributions increase, implying better stability of these species. The existence of oxidized N was previous observed in similar condition from another study.[46] Since there was no oxygen content in PEI, the oxidized nitrogen groups are presumably caused by the addition of KOH. Many research[47,48]

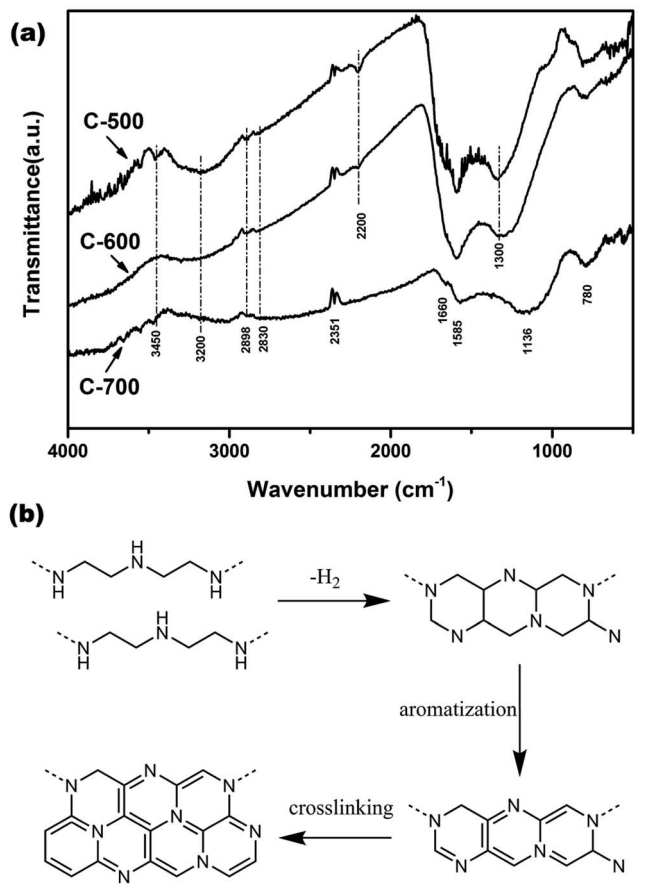

Fig. 4 (a) FT-IR spectrums of PEI-derived carbons at different activation temperatures (curves were displaced vertically in order to be differentiated); (b) hypothesized carbonization of PEI.

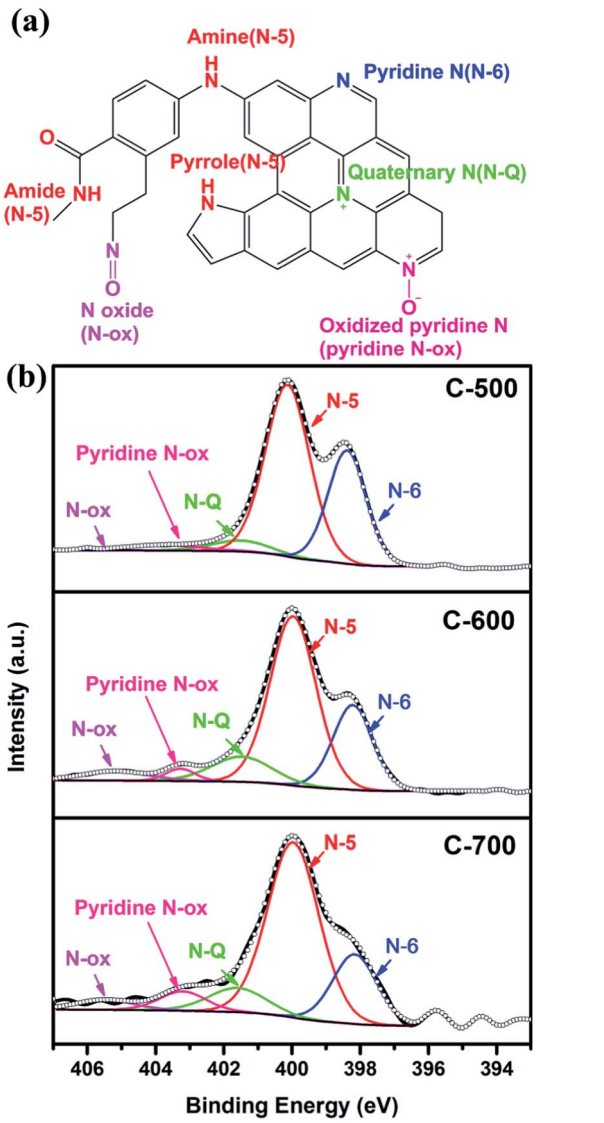

Fig. 5 XPS N 1s spectra of PEI-derived carbons. (a) Schematics of different nitrogen groups on PEI-derived carbons; (b) resolved peaks for samples with different conditions.

Table 2 XPS element content and the contribution of nitrogen species

	XPS element (atomic %)			Nitrogen species contribution (%)				
Sample	C	O	N	N-5	N-6	N-*Q*	Pyridine-N-ox	N-ox
C-500	77.0	11.8	11.1	58.4	33.3	4.9	3.2	0.2
C-600	82.8	10.3	6.9	57.1	24.7	11.1	2.6	4.5
C-700	83.9	13.4	2.7	60.2	20.6	9.3	6.0	3.9

Table 3 CO_2 adsorption capacity of PEI-derived carbons at different temperatures

	CO_2 uptake (mmol g^{-1})			
Sample	0 °C, 1 bar (after HCl neutralization)	0 °C, 0.15 bar (after HCl neutralization)	25 °C, 1 bar	25 °C, 0.15 bar
C-500	4.8(4.2)	2.3(1.8)	2.8	0.9
C-600	5.7(5.2)	2.3(1.9)	3.6	1.0
C-700	5.0(4.5)	1.6(1.4)	2.8	0.6

proposed that with existence of KOH, oxygen is able to link to carbon/sulfur atom in the framework. It is also possible that oxygen could be incorporated into the framework through nitrogen. To conclude, PEI-derived carbons contain various nitrogen functional groups with a majority of N-5. This could be beneficial to CO_2 adsorption, for that many previous studies[22,38,49] claim positive influence of N-containing groups.

3.3 CO_2 adsorption performance

In Table 3, CO_2 adsorption performance of PEI-derived carbons was shown at 0 °C and 25 °C under ambient and sub-ambient pressure (1 bar and 0.15 bar). All the examined samples show good adsorption capacity at 0 °C. C-600 has the highest CO_2 uptake value among the samples, 5.7 mmol g^{-1} at 0 °C 1 bar and 3.6 mmol g^{-1} at 25 °C 1 bar, which are competitive values to some of the N-doped porous carbons recently reported.[22,23,38,50,51] In contrast, C-700 has a similar BET surface area, but achieves less CO_2 uptake (5.0 mmol g^{-1}), which is reasonable because C-700 has less fine microporosity (<1 nm sized pores) and less nitrogen content. Additionally, although C-500 (4.8 mmol g^{-1}) has much smaller BET value than C-700, it has similar CO_2 adsorption results at 1 bar, possibly due to the compensation of rich nitrogen content in C-500. In order to demarcate the contribution of microporosity with N-containing groups, PEI-derived carbons were treated with concentrated HCl (37%) solution in order to neutralize the effect of nitrogen groups. The reduction of CO_2 uptake after acid neutralization is 0.5–0.6 mmol g^{-1} at 1 bar, as shown in Table 3. Based on this, the contribution of N-containing groups is about 9% to 13%. At 0.15 bar, the reduction of CO_2 uptake after acid neutralization is 0.2–0.5 mmol g^{-1}, taking 13% to 23% of the total capacity. An increase of the contribution at lower pressure shows a more significant role of N-containing groups for low-pressure CO_2 adsorption.

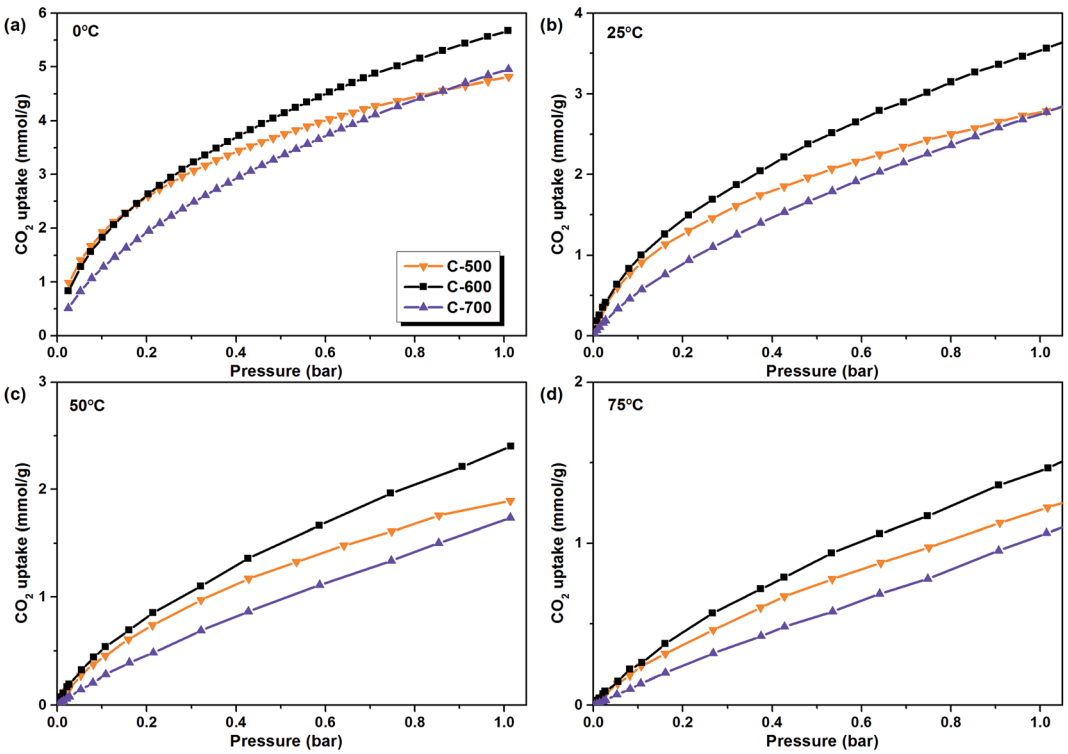

Fig. 6 CO_2 adsorption isotherms of PEI-derived carbons at different temperatures. (a) 0 °C; (b) 25 °C; (c) 50 °C; (d) 75 °C.

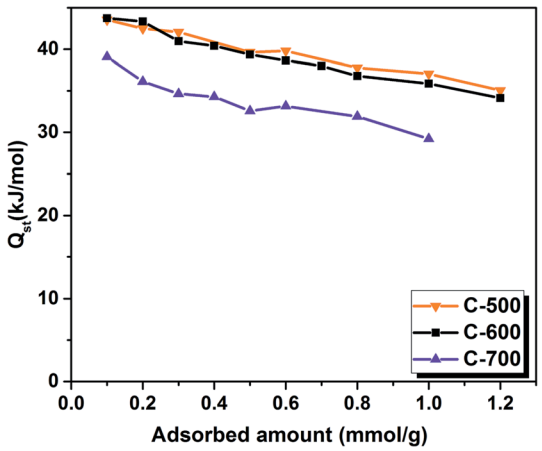

Fig. 7 Isosteric heat of adsorption for PEI-derived carbons.

Isotherms at various temperatures were also presented in Fig. 6. It is observed that as expected, when temperature increases the adsorption capacity drops quickly for all three samples, implying the physisorption nature of the materials. At 0 °C, the capacity at 1 bar is 4.9–5.7 mmol g^{-1}. At 25 °C, it is 2.9–3.7 mmol g^{-1}. When the temperature increases to 75 °C, the uptake is only 1.1–1.5 mmol g^{-1}. What is notable in Fig. 6 is that C-500 has competitive adsorption capacity with C-600 at low pressures (<0.15 bar), but fails to be comparable at near-atmospheric pressure.

In Fig. 7 the isosteric heat of adsorption (Q_{st}) was calculated by applying Clausius–Clayperon equation on isotherms at 0 °C, 25 °C, 50 °C and 75 °C. It could be seen that the initial value of adsorption heat is high, in the range of 39–43 kJ mol^{-1}. This Q_{st} is higher than those of many previously reported nitrogen-rich carbons (30.4–36 kJ mol^{-1} as referred in literatures[22,49]), indicating strong interaction between CO_2 with the sorbent surface. The Q_{st} decreases with increased adsorption amount, revealing that CO_2 adsorption is heterogeneous. This fact emphasizes the important role of N-containing groups in the high initial Q_{st}. Interestingly, C-500 has higher N content than C-600 while they present similar Q_{st} value. This is probably due to a limited access of gas molecule to some of the N-containing groups on C-500 sample, induced by not-well-developed microporosity.

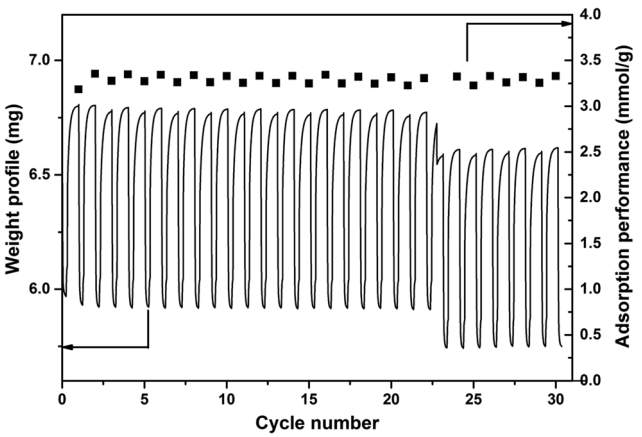

Fig. 8 Stability test (30 cycles) for PEI-derived carbon (C-600) at 25 °C. 1st cycle: 3.18 mmol g^{-1}, 2nd cycle: 3.35 mmol g^{-1}; 30th cycle: 3.32 mmol g^{-1}.

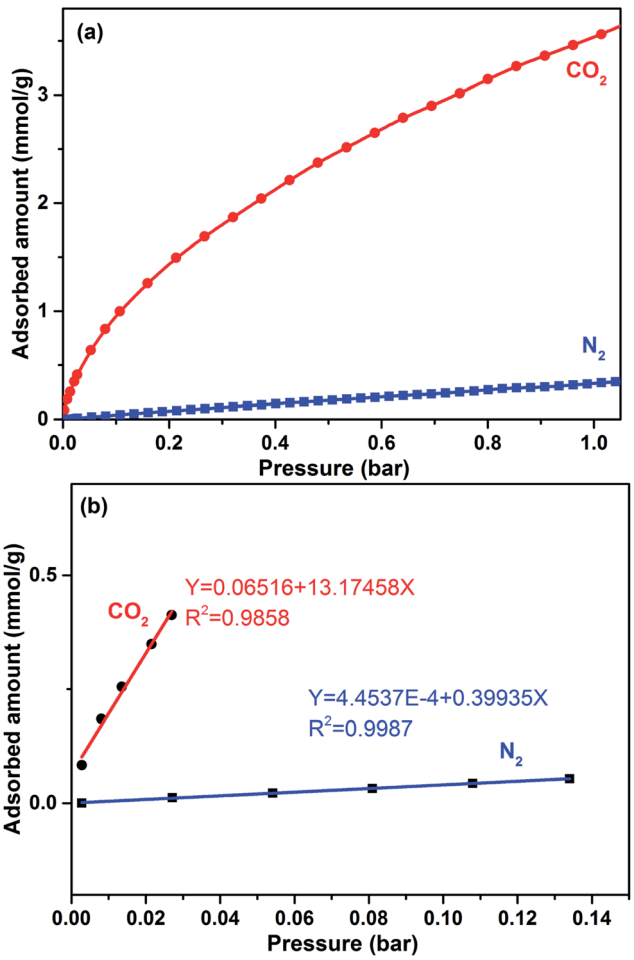

Fig. 9 (a) CO_2 and N_2 isotherms of PEI-derived carbon (C-600) at 25 °C and (b) initial slope for CO_2/N_2 selectivity calculation.

For a cost-efficient adsorbent, the material should also present satisfactory stability during cyclic adsorption–desorption processes. The stability test in Fig. 8 was measured at 25 °C. It shows less than 1% drop (from 2nd cycle, 3.35 mmol g^{-1} to 30th cycle, 3.32 mmol) for C-600 after ~30 cycles, demonstrating a very good stability. This means that the material could be used for long-term purpose and further lowers the cost. Additionally, the selectivity of C-600 at 25 °C was demonstrated in Fig. 9. Fig. 9a shows CO_2 and N_2 isotherms while in Fig. 9b the initial slopes of CO_2 and N_2 isotherms were determined. The selectivity of CO_2 over N_2 was calculated using Henry's law through the initial slopes of the isotherms. Therefore the selectivity of C-600 is 33 at 25 °C, which is also a competitively high value compared to previous report.[22,49,52]

4. Conclusion

A new kind of porous carbon has been successfully synthesized by using a liquid precursor—PEI. The synthesizing process is facile and the resulting carbon possesses well-developed

microporosity and rich nitrogen content (up to 11%). These PEI-derived carbons present good CO_2 adsorption capacity at ambient pressure, up to 5.7 mmol g^{-1} at 0 °C and up to 3.7 mmol g^{-1} at 25 °C. By applying concentrated HCl solution, the contribution of N-containing groups was determined to be 9% to 13% at 1 bar and increases at lower pressure. The initial value of heat of adsorption was measured to be 39–43 kJ mol^{-1}, indicating strong interaction between CO_2 and the sorbent surface. Additionally, the optimized PEI-derived carbons exhibit high multi-cycle adsorption–desorption stability and highly selective adsorption of CO_2 over N_2 at 25 °C demonstrates a very good potential for industrial scale-up application.

Acknowledgements

The authors would like to acknowledge Carbon Management Canada for the financial support and Dr Xinwei Cui for TEM investigation.

References

1 B. P. Spigarelli and S. K. Kawatra, *J. CO_2 Util.*, 2013, **1**, 69–87.
2 M. Nandi and H. Uyama, *Chem. Rec.*, 2014, **14**, 1134–1148.
3 P. D. Vaidya and E. Y. Kenig, *Chem. Eng. Technol.*, 2007, **30**, 1467–1474.
4 R. Banerjee, A. Phan, B. Wang, C. Knobler, H. Furukawa, M. O'Keeffe and O. M. Yaghi, *Science*, 2008, **319**, 939–943.
5 A. Samanta, A. Zhao, G. K. H. Shimizu, P. Sarkar and R. Gupta, *Ind. Eng. Chem. Res.*, 2012, **51**, 1438–1463.
6 E. Kim, T. Lee, H. Kim, W. J. Jung, D. Y. Han, H. Baik, N. Choi and J. Choi, *Environ. Sci. Technol.*, 2014, **48**, 14828–14836.
7 D. X. Wang, X. X. Wang, X. L. Ma, E. Fillerup and C. S. Song, *Catal. Today*, 2014, **233**, 100–107.
8 U. Patil, A. Fihri, A. H. Emwas and V. Polshettiwar, *Chem. Sci.*, 2012, **3**, 2224–2229.
9 L. Wang, M. L. Yao, X. Hu, G. S. Hu, J. Q. Lu, M. F. Luo and M. H. Fan, *Appl. Surf. Sci.*, 2015, **324**, 286–292.
10 Z. J. Zhang, Z. Z. Yao, S. C. Xiang and B. L. Chen, *Energy Environ. Sci.*, 2014, **7**, 2868–2899.
11 G. Srinivas, V. Krungleviciute, Z. X. Guo and T. Yildirim, *Energy Environ. Sci.*, 2014, **7**, 335–342.
12 J. M. Yu and P. B. Balbuena, *ACS Sustainable Chem. Eng.*, 2015, **3**, 117–124.
13 H. Furukawa and O. M. Yaghi, *J. Am. Chem. Soc.*, 2009, **131**, 8875–8883.
14 R. Vaidhyanathan, S. S. Iremonger, G. K. H. Shimizu, P. G. Boyd, S. Alavi and T. K. Woo, *Science*, 2010, **330**, 650–653.
15 D. H. Lin, X. T. Zhang, X. W. Cui and W. X. Chen, *RSC Adv.*, 2014, **4**, 27414–27421.
16 Z. Q. Luo, S. H. Lim, Z. Q. Tian, J. Z. Shang, L. F. Lai, B. MacDonald, C. Fu, Z. X. Shen, T. Yu and J. Y. Lin, *J. Mater. Chem.*, 2011, **21**, 8038–8044.
17 L. F. Wang and R. T. Yang, *J. Phys. Chem. C*, 2012, **116**, 1099–1106.
18 M. Nandi, K. Okada, A. Dutta, A. Bhaumik, J. Maruyama, D. Derks and H. Uyama, *Chem. Commun.*, 2012, **48**, 10283–10285.
19 D. H. Lin, Y. X. Jiang, S. R. Chen, S. P. Chen and S. G. Sun, *Electrochim. Acta*, 2012, **67**, 127–132.
20 M. J. Zhong, S. Natesakhawat, J. P. Baltrus, D. Luebke, H. Nulwala, K. Matyjaszewski and T. Kowalewski, *Chem. Commun.*, 2012, **48**, 11516–11518.
21 M. Zhong, E. K. Kim, J. P. McGann, S. E. Chun, J. F. Whitacre, M. Jaroniec, K. Matyjaszewski and T. Kowalewski, *J. Am. Chem. Soc.*, 2012, **134**, 14846–14857.
22 X. Q. Fan, L. X. Zhang, G. B. Zhang, Z. Shu and J. L. Shi, *Carbon*, 2013, **61**, 423–430.
23 M. Sevilla, P. Valle-Vigon and A. B. Fuertes, *Adv. Funct. Mater.*, 2011, **21**, 2781–2787.
24 M. Sevilla and A. B. Fuertes, *Energy Environ. Sci.*, 2011, **4**, 1765–1771.
25 A. Wahby, J. M. Ramos-Fernandez, M. Martinez-Escandell, A. Sepulveda-Escribano, J. Silvestre-Albero and F. Rodriguez-Reinoso, *ChemSusChem*, 2010, **3**, 974–981.
26 R. T. Wang, P. Y. Wang, X. B. Yan, J. W. Lang, C. Peng and Q. J. Xue, *ACS Appl. Mater. Interfaces*, 2012, **4**, 5800–5806.
27 Y. Liu, D. C. Wu, W. D. Zhang, X. Jiang, C. B. He, T. S. Chung, S. H. Goh and K. W. Leong, *Angew. Chem., Int. Ed.*, 2005, **44**, 4782–4785.
28 M. U. T. Le, S. Y. Lee and S. J. Park, *Int. J. Hydrogen Energy*, 2014, **39**, 12340–12346.
29 X. X. Wang, X. L. Ma, C. S. Song, D. R. Locke, S. Siefert, R. E. Winans, J. Mollmer, M. Lange, A. Moller and R. Glaser, *Microporous Mesoporous Mater.*, 2013, **169**, 103–111.
30 J. Q. Zhao, F. Simeon, Y. J. Wang, G. S. Luo and T. A. Hatton, *RSC Adv.*, 2012, **2**, 6509–6519.
31 W. Yan, J. Tang, Z. J. Bian, J. Hu and H. L. Liu, *Ind. Eng. Chem. Res.*, 2012, **51**, 3653–3662.
32 S. B. Yang, L. Zhan, X. Y. Xu, Y. L. Wang, L. C. Ling and X. L. Feng, *Adv. Mater.*, 2013, **25**, 2130–2134.
33 M. Kruk, M. Jaroniec, R. Ryoo and S. H. Joo, *J. Phys. Chem. B*, 2000, **104**, 7960–7968.
34 K. S. W. Sing, D. H. Everett, R. A. W. Haul, L. Moscou, R. A. Pierotti, J. Rouquerol and T. Siemieniewska, *Pure Appl. Chem.*, 1985, **57**, 603–619.
35 X. Hu, M. Radosz, K. A. Cychosz and M. Thommes, *Environ. Sci. Technol.*, 2011, **45**, 7068–7074.
36 N. P. Wickramaratne and M. Jaroniec, *Adsorption*, 2014, **20**, 287–293.
37 J. T. Wang, H. C. Chen, H. H. Zhou, X. J. Liu, W. M. Qiao, D. H. Long and L. C. Ling, *J. Environ. Sci.*, 2013, **25**, 124–132.
38 G. P. Hao, W. C. Li, D. Qian and A. H. Lu, *Adv. Mater.*, 2010, **22**, 853–857.
39 X. T. Zhang, J. Zhang, W. H. Song and Z. F. Liu, *J. Phys. Chem. B*, 2006, **110**, 1158–1165.
40 D. H. Lin, Y. X. Jiang, Y. Wang and S. G. Sun, *J. Nanomater.*, 2008, DOI: 10.1155/2008/473791.
41 X. X. Wang, V. Schwartz, J. C. Clark, X. L. Ma, S. H. Overbury, X. C. Xu and C. S. Song, *J. Phys. Chem. C*, 2009, **113**, 7260–7268.

42 P. J. Larkin, *Infrared and Raman Spectroscopy: Principles and Spectral Interpretation*, 2011, pp. 1–228.
43 H. L. Spell, *Anal. Chem.*, 1969, **41**, 902–905.
44 C. Weidenthaler, A. H. Lu, W. Schmidt and F. Schuth, *Microporous Mesoporous Mater.*, 2006, **88**, 238–243.
45 R. Pietrzak, *Fuel*, 2009, **88**, 1871–1877.
46 B. Kumar, M. Asadi, D. Pisasale, S. Sinha-Ray, B. A. Rosen, R. Haasch, J. Abiade, A. L. Yarin and A. Salehi-Khojin, *Nat. Commun.*, 2013, **4**, DOI: 10.1038/ncomms3819.
47 S. H. Lee and C. S. Choi, *Fuel Process. Technol.*, 2000, **64**, 141–153.
48 N. Yoshizawa, K. Maruyama, Y. Yamada, E. Ishikawa, M. Kobayashi, Y. Toda and M. Shiraishi, *Fuel*, 2002, **81**, 1717–1722.
49 Y. D. Xia, R. Mokaya, G. S. Walker and Y. Q. Zhu, *Adv. Energy Mater.*, 2011, **1**, 678–683.
50 C. Pevida, T. C. Drage and C. E. Snape, *Carbon*, 2008, **46**, 1464–1474.
51 L. Liu, Q. F. Deng, T. Y. Ma, X. Z. Lin, X. X. Hou, Y. P. Liu and Z. Y. Yuan, *J. Mater. Chem.*, 2011, **21**, 16001–16009.
52 C. Chen, J. Kim and W. S. Ahn, *Fuel*, 2012, **95**, 360–364.